Reconstruction of cone-beam projections from Compton scattered data [1]

Lucas C. Parra,
Sarnoff Corporation, CN 5300, Princeton, New Jersey 08543

Abstract

The problem of reconstructing a 3D source distribution from Compton scattered data can be separated into two tasks. First, the angular distribution of line projections at different observation points within the detector volume are reconstructed. Then, reconstruction techniques are applied to the resulting cone-beam projections to synthesize the 3D source distribution. This paper describes an analytic solution for the first, yet unsolved, task. Building on the convolution theorem in spherical coordinates, a back-projection and inverse filtering technique in terms of spherical harmonics is formulated. The rotation invariance of the point response of the back-projection in spherical coordinates is proved; and the corresponding inverse filter function is derived. The resulting filtered back-projection algorithm then consists of a summation over all detected events of fixed and known event response functions. Measurement errors, which for Compton scatter detectors are typically different for each detected event, can easily be accounted for in the proposed algorithm. The computational cost of the algorithm is $O(NT^2)$, where N is the number of detected events and π/T is the desired angular resolution.

I. Introduction

The use of Compton scatter events for imaging in nuclear medicine was first proposed in [1]. The information collected in a Compton event includes the location where a primary γ-quantum is scattered, the energy transferred to a recoil electron, and the direction of the Compton scattered secondary γ-quantum. A scatter angle can be computed from the transferred energy; thus, for a given event, the origin of the primary quantum can be determined to lie somewhere on a cone-surface (see Figure 1). This technique is sometimes referred to as electronic collimation [2, 3, 4, 5], because measurement of the scatter angle, in a sense, acts as a collimator in determining the direction of arrival. There are trade-offs in using electronic collimation rather than a mechanical collimator. Electronic collimation using Compton scatter holds the promise of a much larger event count [6]; however each event will contain less information, since the origin of the primary quantum can only be determined to lie within a cone-surface, rather than along a line, as with a physical collimator. Lack of a physical collimator further complicates reconstruction because without a physical collimator, angular resolution due to measurement errors can vary from event to event.

[1]This work was mostly developed during 1995 while working at the Imaging Department of Siemens Corporate Research, 755 College Road East, Princeton, NJ 08540

Various approaches have been proposed to compute the generating 3D source distribution from a collection of scattered Compton events. A pioneer in the concept of the Compton camera, Singh, has presented a series of reconstruction methods mainly concerned with numerical methods like ML, EM, ART, etc. [5, 4]. These algorithms, in general, require binning of the data. However, due to the dimensionality of the measurement space (six dimensions) this may not be an optimal approach. Instead, event-based reconstruction techniques which avoid binning, at least in some coordinates, may be preferable. Along these lines, [7, 8] present, in the context of PET, a general list-mode maximum likelihood estimation algorithm which is well-suited to both the dimensionality and to the measurement errors in the Compton scatter measurement space.

Analytic, rather than numeric solutions have also been proposed to solve the 3D source reconstruction problem [9, 10, 11]. In all instances, the problem is separated into two steps. First, cone-beam or plane projections of the source at different observations points within the detector volume are reconstructed from the measured data. Then synthesis techniques from the field of Computed Tomography are applied to the resulting projections to generate the 3D source distribution. Cree and Bones [10] have developed an analytic expression for direct reconstruction, by severely limiting the accepted events to only those with secondary γ-quanta perpendicular to a detector array. Basko et al. [11] use spherical harmonics to convert cone-surface projections into plane projections; however, they ignore the dependency of the scatter likelihood on the scatter angles given by the Klein-Nishina distribution, and therefore fail to account for a crucial property of Compton scatter.

In this paper we suggest a similar two-step approach to the 3D source reconstruction problem. In the first step we use spherical harmonics to recover cone-beams from cone-surface projections. In contrast to [11], our method does not require costly decomposition into spherical harmonics during reconstruction. Instead, motivated by the work of Krzyzanowski [9], we use the deconvolution in spherical coordinates [2], to obtain a filtered back-projection technique which generates the cone-beam projections directly from the Compton scattered data. The inverse point-spread function in spherical harmonics, (referred to as the *event response function*) is fixed and can be computed prior to reconstruction. To compute the 3D source distribution from the projections, we propose cone-beam reconstruction techniques [12, 13, 14, 15]; these are admittedly more complex than the simple Radon inversion used in [11]. Our algorithm goes beyond previous approaches in that it accounts for measurement errors which

[2]The spherical deconvolution equation is derived in Appendix A.

0018-9499/00$10.00

vary from event to event (an additional difficulty that arises for any real Compton scatter detectors).

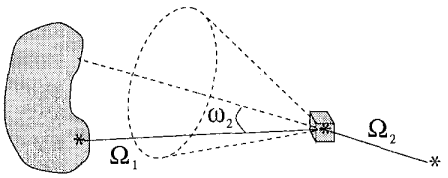

Figure 1: Cone surface projection of a Compton scattering event. Positions indicated with an * represent locations of an emission of primary quantum, location of scatter, and detection of the secondary quantum. The orientations of the primary and secondary quanta are Ω_1 and Ω_2, respectively. The location of the scattering event, the absorption of the secondary quantum, and the scatter angle ω_2 can be measured, and together determine the origin point of the emission of the primary quantum to lie within the cone-surface shown. Reconstruction for events scattered in a given volume element will be considered.

In Section II the idealized imaging process for a given scattering volume element in the detector is derived, i.e., the transformation from cone-beam projections to cone-surface projections. In Section III we demonstrate that this process represents a convolution in spherical coordinates; and we introduce the inversion of such a spherical convolution using spherical harmonics. In Section IV the back-projection of a cone-surface projection is presented, and the rotation invariance of the overall transfer function, from cone-beam projections to summation image, is demonstrated. The resulting summation image can then be inverted with a spherical deconvolution. Finally, in Section V the back-projection and inverse filtering are combined into a single filtered back-projection procedure. The resulting algorithm is used to reconstruct a simple source distribution from simulated Compton data in section VI. Appendix A derives the convolution theorem for spherical harmonics; and the corresponding deconvolution with Legendre polynomials is derived in Appendix B.

II. Measurements and Image Generation

Consider a particular volume element of a detector where Compton scattering events are being observed (see Figure 1). Our discussion throughout this paper will focus on such a single volume element in the detector. A particular direction from which primary γ-quanta originate can be described by the angles φ_1, (azimuth), and ϑ_1 (elevation). Using Ω_1 to denote the angle pair (φ_1, ϑ_1), the density of the γ-quanta detected from direction Ω_1 is denoted by $g(\Omega_1)$. Thus, $g(\Omega_1)$ gives the projection of the three dimensional source distribution along the line which intersects the volume element from direction Ω_1; i.e., $g(\Omega_1)$ gives the *cone-beam projections*. A Compton camera measures the directions Ω_2 of the scattered secondary γ-quanta. By also measuring the energy E_e of the recoil electron, the kinematics of Compton scattering gives us the scatter angle ω_2,

$$\cos\omega_2 = 1 - \frac{E_e}{\gamma(h\nu - E_e)}\,, \tag{1}$$

where $\gamma = h\nu/m_ec^2$, $h\nu$ is the energy of the primary γ-quantum and $m_ec^2 = 511keV$ [16]. The Compton camera therefore collects an image intensity distribution $f(\varphi_2, \vartheta_2, \omega_2)$ over three angles for every volume element in the detector. (Issues related to measurement errors will be ignored for now, and will be addressed in Sections IV and V.)

To derive an analytic solution to the reconstruction problem, we must first derive an expression that describes how a measured image $f(\varphi_2, \vartheta_2, \omega_2)$ generates from a given angular distribution of line projections $g(\Omega_1)$. Let $p(\Omega_2, \omega_2|\Omega_1)$ denote the probability density of making the observation Ω_2, ω_2, given that the event originated from direction Ω_1. We can then write:

$$f(\Omega_2, \omega_2) = \int d\Omega_1 p(\Omega_2, \omega_2|\Omega_1) g(\Omega_1)\,. \tag{2}$$

Denoting the angle $\angle\Omega_1\Omega_2 = \omega$, and the azimuth with φ, such that $d\Omega_1 = d\varphi d(\cos\omega)$, we can write:

$$\begin{aligned} p(\Omega_2, \omega_2|\Omega_1) &= p(\omega, \varphi, \omega_2) && (3)\\ &= (2\pi)^{-1} p(\omega, \omega_2) && (4)\\ &= (2\pi)^{-1} p(\omega_2|\omega) p(\omega) && (5)\\ &= (2\pi)^{-1} \delta(\cos\omega_2 - \cos\omega) p(\omega)\,. && (6) \end{aligned}$$

For Eq. (3) we have assumed that the scatter distribution does not depend on the absolute direction of the incident quantum, and in Eq. (4) it is assumed that it is independent of the azimuth. Both of these assumptions are strictly met by Compton scatter. However, depending on the detector geometry, note that these assumptions may be invalid in some regions of the detector, due to boundary effects.

The probability distribution $p(\omega)$ of measuring an event with scatter angle ω is proportional to the differential cross-section, $h(\cos\omega)$

$$p(\omega) \propto \frac{d\sigma}{d\Omega_2} \propto h(\cos\omega)\,; \tag{7}$$

and variations in detector efficiency as a function of scatter angle or position in detector volume (arising from detector architecture) can be accounted for in the definition of $h(\cos\omega)$.

Given $h(\cos\omega)$, Eq.(2) for image formation now becomes:

$$f(\Omega_2, \omega_2) = \int d\Omega_1 g(\Omega_1) h(\cos\omega) \delta(\cos\omega_2 - \cos\omega)\,. \tag{8}$$

The proportionality factor $\left(2\pi \int d(\cos\omega) h(\cos\omega)\right)^{-1}$ can be absorbed into the definition of f or g. In order to reconstruct for every point in the detector volume, the distribution of line projections $g(\Omega_1)$ from the measured data $f(\Omega_2, \omega_2)$, Eq.(8) must be inverted. Given $g(\Omega_1)$ for a manifold of scatter points, a cone-beam projection algorithm can then be used to recover the 3D source distribution.

III. Spherical Deconvolution

First consider the measured image intensity $f(\Omega_2, \omega_2)$ summed over all measured scatter angles ω_2:

$$f(\Omega_2) = \int d(cos\omega_2) f(\Omega_2, \omega_2). \tag{9}$$

Applying this integration to Eq. (8) we obtain:

$$f(\Omega_2) = \int d\Omega_1 g(\Omega_1) h(\cos\omega)\,. \qquad (10)$$

This integration can be performed analytically by applying the following spherical trigonometry relation between Ω_1 and Ω_2:

$$\cos\omega = \cos\vartheta_1 \cos\vartheta_2 + \sin\vartheta_1 \sin\vartheta_2 cos(\varphi_1 - \varphi_2)\,. \qquad (11)$$

Eq.(10) can be interpreted as a convolution in the spherical coordinate space, with convolution kernel $h(\cos\omega)$. Since the convolution kernel depends only on the angular distance between Ω_1 and Ω_2, this integral equation is shift invariant in the angular space (rotationally invariant). Furthermore, it can be shown (see Appendix A) that, by expanding both sides of equation (10) in the appropriate system of orthogonal basis functions, the right side of Eq.(10) is transformed into a product. This is analogous to the convolution theorem in Cartesian coordinates.

In this context, the following deconvolution formula can be derived (see Appendix B):

$$g(\Omega_1) = \int d\Omega_2 f(\Omega_2) h^{-1}(\cos\omega)\,, \qquad (12)$$

where

$$h^{-1}(\cos\omega) = \sum_{n=0}^{\infty} \left(\frac{2n+1}{4\pi}\right)^2 \frac{P_n(\cos\omega)}{H_n}\,, \qquad (13)$$

the expansion coefficients H_n are given by

$$H_n = \frac{2n+1}{2} \int d(\cos\omega) h(\cos\omega) P_n(\cos\omega), \qquad (14)$$

and the basis functions $P_n(\cos\omega)$ are Legendre polynomials. This deconvolution formula can be used to reconstruct the distribution of line projections $g(\Omega_1)$.

However, in employing Eq.(13), we encounter a difficulty typical in inverse filtering: the presence of the expansion coefficients H_n in the denominator. To avoid instability, these coefficients must be significantly different from zero. Unfortunately, as seen in Figure 2, the inverse of the convolution kernel corresponding to the differential cross-section of Compton scatter (cf. Eq. (29)) will have some vanishing expansion coefficients. In fact, only the first few coefficients give finite values.

To solve this problem, inverse filtering techniques suggest generation of a summation image by back projection of the measured events [17]. The summation image of the back-projections usually satisfies a linear convolution like that in Eq.(10). Once the overall transfer function from source to summation image has been computed, one can use inverse filtering according to Eqs. (12)-(14).

IV. Back-projection and inverse filtering

The main problem confronted in the angular reconstruction is ambiguity in the event measurements. A particular event

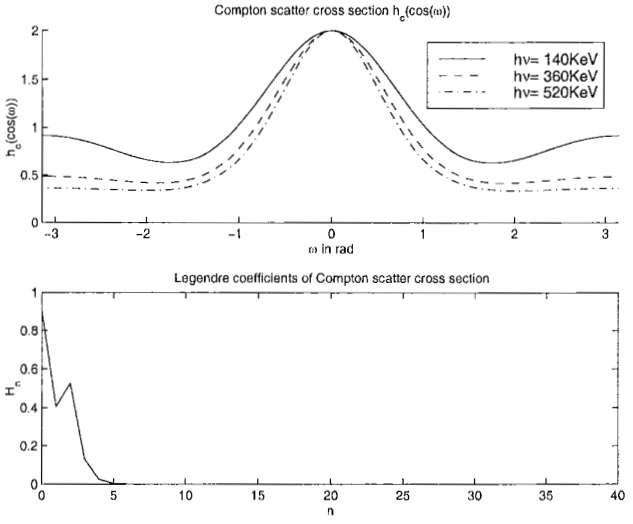

Figure 2: Top: differential cross section $h_c(\omega)$ of Compton scattering given in Eq. (29) for three primary quantum Energies $140keV$, $360keV$ and $511keV$. Bottom: First 40 corresponding expansion coefficients H_n^c in the base of Legendre polynomials, plotted only for $140keV$

measured at coordinates Ω_2, ω_2 could have originated from any direction Ω_1, so long as Ω_1 forms an angle ω_2 with Ω_2. This set of possible directions form a cone-surface of ambiguity. *Back-projection* entails assigning to all directions Ω_1' which might have contributed to a particular $f(\Omega_2, \omega_2)$, the same image intensity: $f(\Omega_2, \omega_2)\delta(\cos\omega_2 - \cos\omega')$, where $\omega' = \angle\Omega_1'\Omega_2$. Back-projections here refer to projecting back all cones with their vertex laying within a single volume element as indicated in figure 3.

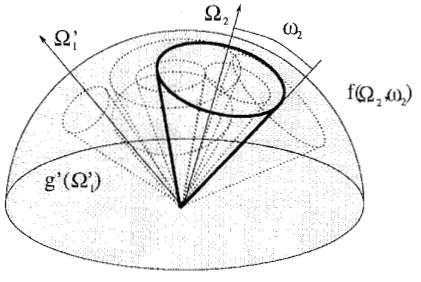

Figure 3: The summation image $g'(\Omega_1')$ (shaded) can be interpreted as summing intensities $f(\Omega_2, \omega_2)$ (bold) onto the unit sphere along circles with center Ω_2 and opening ω_2.

The corresponding *summation image* $g'(\Omega_1')$ of the back-projections is defined as:

$$g'(\Omega_1') = \int d(\cos\omega_2) \int d\Omega_2 f(\Omega_2, \omega_2)\delta(\cos\omega_2 - \cos\omega')\,. \qquad (15)$$

We will now demonstrate that the summation image can be expressed by an angular convolution of the line projections $g(\Omega_1)$ with an appropriate point spread function. This can then

be used to reconstruct $g(\Omega_1)$ from $g'(\Omega_1')$ by means of the deconvolution of Eq.(12).

First we will calculate the overall response function for a point-like distribution in angular space, that is, the *point spread function* of the scatter plus back-projection. The original distribution of line projections is given by $g_{\Omega_1^*}(\Omega_1) = \delta(\cos\vartheta_1 - \cos\vartheta_1^*)\delta(\varphi_1 - \varphi_1^*)$. The index Ω_1^* denotes that this is a particular distribution corresponding to an angular point located at Ω_1^*. Inserting this into Eq.(8) one obtains the observable distribution $f_{\Omega_1^*}(\Omega_2, \omega_2)$:

$$
\begin{aligned}
& f_{\Omega_1^*}(\Omega_2, \omega_2) \\
&= \int d(\cos\vartheta_1) d\varphi_1 \delta(\cos\vartheta_1 - \cos\vartheta_1^*)\delta(\varphi_1 - \varphi_1^*) \\
&\quad h(\cos\omega)\delta(\cos\omega - \cos\omega_2) \qquad (16) \\
&= \int d(\cos\vartheta_1) d\varphi_1 \delta(\cos\vartheta_1 - \cos\vartheta_1^*)\delta(\varphi_1 - \varphi_1^*) \\
&\quad h(\cos\vartheta_1\cos\vartheta_2 + \sin\vartheta_1\sin\vartheta_2\cos(\varphi_1 - \varphi_2)) \\
&\quad \delta(\cos\vartheta_1\cos\vartheta_2 + \sin\vartheta_1\sin\vartheta_2\cos(\varphi_1 - \varphi_2) - \cos\omega_2) \qquad (17) \\
&= h(\cos\vartheta_1^*\cos\vartheta_2 + \sin\vartheta_1^*\sin\vartheta_2\cos(\varphi_1^* - \varphi_2)) \\
&\quad \delta(\cos\vartheta_1^*\cos\vartheta_2 + \sin\vartheta_1^*\sin\vartheta_2\cos(\varphi_1^* - \varphi_2) - \cos\omega_2) \qquad (18) \\
&= h(\cos\omega^*)\delta(\cos\omega^* - \cos\omega_2)\,, \qquad (19)
\end{aligned}
$$

where Eq.(11) for ω, and the analogous expression for $\omega^* = \angle\Omega_1^*\Omega_2$ have been used. Inserting this result into Eq.(15) one obtains the desired point spread function in the summation image:

$$
\begin{aligned}
g'_{\Omega_1^*}(\Omega_1') &= \int d(\cos\omega_2) \int d\Omega_2 h(\cos\omega^*) \\
&\qquad \delta(\cos\omega^* - \cos\omega_2)\delta(\cos\omega_2 - \cos\omega') \qquad (20) \\
&= \int d\Omega_2 h(\cos\omega^*)\delta(\cos\omega^* - \cos\omega')\,. \qquad (21)
\end{aligned}
$$

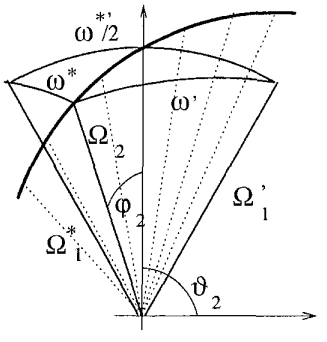

Figure 4: The bold solid line shows the path along which the integration (with respect to Ω_2) for h_{bp} in Eq.(21) is performed.

Since the integral (21) must be calculated for a fixed set of angles Ω_1^*, Ω_1', we may adapt the coordinate system for the integration parameters $\Omega_2 = \varphi_2, \vartheta_2$ as follows. Let the direction that divides the angle between Ω_1^* and Ω_1' be the axis of reference for measuring azimuth angles such as φ_2 (vertical arrow in Figure 4). Let the axis orthogonal to that, and coplanar with Ω_1^* and Ω_1' be the axis of reference for measuring elevation angles such as ϑ_2 (horizontal arrow in Figure 4). For this choice of coordinate frame we have $\varphi^* = \varphi' = 0$, $\vartheta_1^* = \pi/2 + \omega'^*/2$ and $\vartheta_1' = \pi/2 - \omega'^*/2$. The δ-function in Eq.(21) limits the integration to a fixed $\vartheta_2 = \pi/2$ and arbitrary $\varphi_2 \in [0, 2\pi]$. Inserting this into the relations for $\cos\omega^*$ and $\cos\omega'$ in Eq.(11) we obtain:

$$
\delta(\cos\omega^* - \cos\omega') = \delta(\cos\vartheta_2 2\sin\frac{\omega'^*}{2}) = \frac{\delta(\cos\vartheta_2)}{2\sin\frac{\omega'^*}{2}}\,. \qquad (22)
$$

Now integration over ϑ_2 can be performed easily:

$$
\begin{aligned}
g'_{\Omega_1^*}(\Omega_1') &= \int d(\cos\vartheta_2) d\varphi_2 h(\cos\omega^*) \frac{\delta(\cos\vartheta_2)}{2\sin\frac{\omega'^*}{2}} \qquad (23) \\
&= \frac{1}{2\sin\frac{\omega'^*}{2}} \int_0^{2\pi} d\varphi_2 h(\sin\vartheta^*\cos(\varphi_2)) \qquad (24) \\
&= \frac{1}{\sqrt{1 - \cos^2\frac{\omega'^*}{2}}} \int_{-\cos\frac{\omega'^*}{2}}^{\cos\frac{\omega'^*}{2}} dz \frac{h(z)}{\sqrt{\cos^2\frac{\omega'^*}{2} - z^2}} \qquad (25) \\
&= h_{\mathrm{bp}}(\cos\omega'^*)\,. \qquad (26)
\end{aligned}
$$

Note that the integration above produces a function $h_{bp}(\cos\omega'^*)$ which depends only on the angle $\omega'^* = \angle\Omega_1'\Omega_1^*$ between the orientation of the angular point source Ω_1^* and the observation point Ω_1' in the summation image; $h_{bp}(\cos\omega'^*)$ is shift invariant in the angular space. The summation image point spread function is shown in Figure 5.

An arbitrary source distribution $g(\Omega_1)$ can be understood as a linear superposition of point sources located at Ω_1 and weighting $g(\Omega_1)$. A point source generates in the summation image the point spread function $h_{bp}(\cos\omega_1)$, where $\omega_1 = \angle\Omega_1\Omega_1'$. The summation image of the distribution $g(\Omega_1)$ is then a linear superposition of point spread function $h_{bp}(\cos\omega_1)$ with weighting $g(\Omega_1)$:

$$
g'(\Omega_1') = \int d\Omega_1 g(\Omega_1) h_{\mathrm{bp}}(\cos\omega_1)\,, \qquad (27)
$$

This is now a convolution of the form of Eq.(10), and can be inverted by the deconvolution described in Eqs. (12)-(14) as follows:

$$
g(\Omega_1) = \int d\Omega_1' g'(\Omega_1') h_{\mathrm{bp}}^{-1}(\cos\omega_1)\,. \qquad (28)
$$

The corresponding expansion coefficients H_n^{bp} of the Legendre polynomial decomposition can be calculated numerically, at fairly low computational cost, since they need to be calculated only once.

For unrestricted Compton scatter, the differential cross-section $h(\cos\omega)$ convolution kernel of Eq.(23) is given by the Klein-Nishina distribution [16] (shown in Figure 2):

$$
h(\cos\omega) = h_{\mathrm{c}}(\cos\omega)\frac{1 + \cos^2\omega + \frac{\gamma^2(1-\cos\omega)^2}{1+\gamma(1-\cos\omega)}}{(1 + \gamma(1 - \cos\omega))^2}\,, \qquad (29)
$$

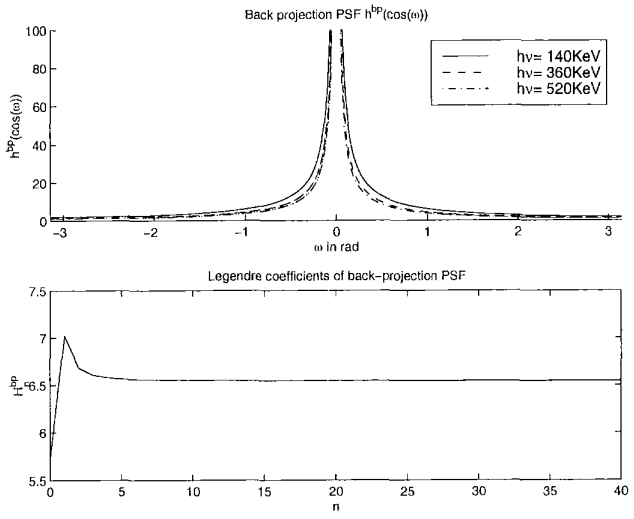

Figure 5: Top: Point spread function h_{bp} in the angular summation image for three different primary quantum Energies $140keV$, $360keV$ and $520keV$. Bottom: First 40 expansion coefficients H_n^{bp} in the base of Legendre polynomials, plotted only for $140keV$. With this coefficients the deconvolution kernel h_{bp}^{-1} for the inverse filtering can be calculated.

Surprisingly, even for this complex form for $h(\cos\omega)$, the resulting integral can be computed in closed form; however, for simplicity, this computation will be omitted here. In Figure 5 it can be seen that for the Compton scatter the H_n^{bp} converge after a few coefficients to a constant value. Fortunately, now they are non-zero and the convolution in Eq. (27) can easily be inverted using the deconvolution kernel defined as in Eq. (13). Given a convolution kernel $h(\cos\omega)$ chosen to account for detector geometry and sensitivity, the integral in Eq.(23) can be computed numerically. This computation could be performed once off-line, before reconstruction.

A few remarks concerning measurement error are in order. In principle, it is possible to include measurement errors in the point spread function h_{bp}. To achieve this, one must convolve $f_{\Omega_1^*}(\Omega_2,\omega_2)$ with a measurement error density representing the detector accuracy, e.g., the product of zero mean normal distributions with standard deviations $\Delta\vartheta_2, \Delta\varphi_2$, and $\Delta\omega_2$. Since $h_{\mathrm{c}}(\cos\omega^*)$ is a slowly varying function it is conceivable that, for small measurement errors, this convolution result could be reasonably approximated in Eq.(19), by replacing the $\delta()$ function by a zero mean normal with standard deviation $\sqrt{\Delta\vartheta_2^2+\Delta\omega_2^2}$. The same substitution would follow in Eq.(23). The resulting integrals can then be computed for the particular detector architecture once, if not analytically, then numerically. This may be in particular needed when including more realistic noise models such as Doppler broadening discussed in detail in [6].

The net effect of this substitution on the point spread function h_{bp} is an added spread of $\sqrt{\Delta\vartheta_2^2+\Delta\omega_2^2}$. As a result, the corresponding expansion coefficients H_n^{bp} are somewhat modified for small n, and vanish for n larger than the angular resolution $T=\pi/\sqrt{\Delta\vartheta_2^2+\Delta\omega_2^2}$. The inversion procedure remains the same, but uses the modified expansion coefficients, determined for the particular detector architecture and accuracy. Due to the vanishing coefficients at higher orders, the inversion has to be low-pass limited. In this way the resolution of the recovered cone-beam projections is limited by the measurement errors.

V. Filtered back-projection

The procedure described in the previous section for reconstructing cone-beam projections from Compton cone-surface projections consists of generation of a summation image, followed by spherical deconvolution. The deconvolution can be performed either directly in the angular space, or by transforming into the spherical harmonics domain, then filtering, then inverse transforming.

It is possible, however, to combine the back-projection of Eq.(15) and the deconvolution of Eq.(28) into the following single filtered back-projection step that will recover the cone-beam projection for a single vertex point:

$$g(\Omega_1) = \int d\Omega_1' g'(\Omega_1') h_{\mathrm{bp}}^{-1}(\cos\omega_1) \tag{30}$$

$$= \int d\Omega_1' \int d(\cos\omega_2) \int d\Omega_2 \; f(\Omega_2,\omega_2)\delta(\cos\omega_2-\cos\omega')h_{\mathrm{bp}}^{-1}(\cos\omega_1) \tag{31}$$

$$= \int d(\cos\omega_2) \int d\Omega_2 f(\Omega_2,\omega_2) \int d\Omega_1' \; \delta(\cos\omega_2-\cos\omega') \; h_{\mathrm{bp}}^{-1}(\cos\vartheta_1\cos\vartheta_1' + \sin\vartheta_1\sin\vartheta_1'\cos(\varphi_1-\varphi_1')) \tag{32}$$

$$= \int d(\cos\omega_2) \int d\Omega_2 f(\Omega_2,\omega_2) \int d\varphi_1' \; h_{\mathrm{bp}}^{-1}(\cos\omega\cos\omega_2 + \sin\omega\sin\omega_2\cos(\varphi_1-\varphi_1')) \tag{33}$$

$$= \int d(\cos\omega_2) \int d\Omega_2 f(\Omega_2,\omega_2) R(\omega,\omega_2)\,. \tag{34}$$

For the integration over ϑ_1' on line (32), the z-axis has been chosen to point in the Ω_2 direction. Then $\vartheta_1=\omega, \vartheta_1'=\omega'$, and integration of the δ-function replaces ω' by ω_2. We refer to the function $R(\omega,\omega_2)$ as the *event response* of a Compton event.

The integration in $R(\omega,\omega_2)$ over φ_1' can be performed analytically as follows:

$$R(\omega,\omega_2) = \int d\varphi_1' h_{\mathrm{bp}}^{-1}(\cos\omega\cos\omega_2+\sin\omega\sin\omega_2\cos(\varphi_1-\varphi_1')) \tag{35}$$

$$= \sum_{n=0}^{\infty}\left(\frac{2n+1}{4\pi}\right)^2 \frac{1}{H_n^{\mathrm{bp}}} \int d\varphi_1' \; P_n(\cos\omega\cos\omega_2+\sin\omega\sin\omega_2\cos(\varphi_1-\varphi_1')) \tag{36}$$

$$= \sum_{n=0}^{\infty} \left(\frac{2n+1}{4\pi}\right)^2 \frac{1}{H_n^{\rm bp}} \int d\varphi_1' \left(\frac{4\pi}{2n+1}\right) \sum_{m=-n}^{n} Y_{nm}^*(\omega_2\varphi_1') Y_{nm}(\omega\varphi_1) \quad (37)$$

$$= \sum_{n=0}^{\infty} \left(\frac{2n+1}{4\pi}\right)^2 \frac{2\pi}{H_n^{\rm bp}} P_n(\cos\omega_2) P_n(\cos\omega) \,. \quad (38)$$

An expansion of the Legendre polynomials in terms of spherical harmonics is used in line (37); and the integration leading to line (38) uses the definition of spherical harmonics (see Eqs. (50) and (42) in Appendix A). For a measured distribution having bandwidth T, the summation over n can be truncated at T. (See Eq.(49) in Appendix A.)

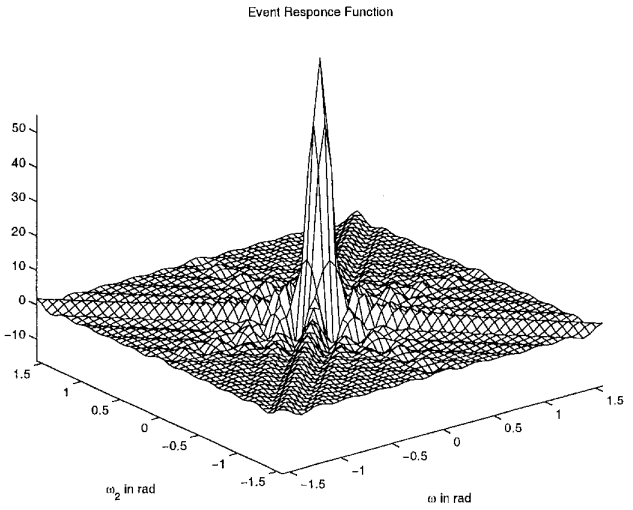

Figure 6: The event response function $R(\omega, \omega_2)$, calculated with expansion coefficients $H_n^{\rm bp}$, for primary quantum energy $140keV$. The expansion has been truncated at order $T = 20$.

In practice, image intensity $f(\Omega_2, \omega_2)$ will be measured at a set of N data points: $(\varphi_2^1, \vartheta_2^1, \omega_2^1), ..., (\varphi_2^N, \vartheta_2^N, \omega_2^N)$. The image intensity can therefore be expressed as a sum of δ-functions at the measurement points: $f(\Omega_2, \omega_2) = \sum_\nu \delta(\varphi_2 - \varphi_2^\nu)\delta(\cos\vartheta_2 - \cos\vartheta_2^\nu)\delta(\cos\omega_2 - \cos\omega_2^\nu)$.

Substituting this expression for $f(\Omega_2, \omega_2)$ into Eq.(34), we obtain for the reconstructed cone-beam projection $g(\Omega_1)$:

$$g(\Omega_1) = \int d(\cos\omega_2) \int d\Omega_2 f(\Omega_2, \omega_2) R(\omega, \omega_2) \quad (39)$$

$$= \sum_{\nu=1}^{N} R(\omega^\nu, \omega_2^\nu) \,. \quad (40)$$

Finally, we assign each event a response function on the angular space Ω_1, parameterized by the measured scatter angle ω_2. Summing these response functions for each event yields the filtered back-projection reconstruction.

As outlined at the end of the previous section, angular resolution π/T is limited by measurement error. Therefore, it is reasonable to truncate the sum in Eq.(38) at $n = T$; and thus in the reconstruction of Eq.(40), only $2T$ bins are needed for each of the angles ϑ_1, and φ_1. As a result, the overall computational cost is $O(NT^2)$, if the event response function has been computed prior to reconstruction.

A serious complication in practical implementations of Compton scattering detectors is that every measured event can have associated with it a different measurement error. The accuracy with which the scatter angle ω_2 can be determined in general depends on the absolute value of the energy ΔE_e of the recoil electron; and furthermore, the precision of Ω_2 depends on the distance of scatter location and absorption.

The filtered back-projection procedure we have proposed in this section has considerable advantages with regards to these difficulties. In the back-projection and filtering technique outlined in the previous section, only *fixed* measurement errors can be considered. In contrast, with the technique described in this section we are free to use different event response functions for every event, with different coefficients $H_n^{\rm bp}$ computed for different measurement errors. If storing different event response functions for all possible measurement errors at the corresponding resolutions is too expensive, one may instead precompute the $H_n^{\rm bp}$ coefficients only for different errors, and then compute the sum in Eq.(40) for every event. The computational cost of the filtered back-projection algorithm then rises to $O(NT^3)$.

VI. Simulations

The algorithm described in the previous sections has been used to reconstruct a simple source distribution from simulated data. The present simulation is intended to demonstrate the recovery of cone-beam projections from Compton scattered data. In order to see the recovered source distribution beyond the Poison noise level and the ambiguity of the cone-surface projections we simulated a large number of events, in the order of 10^5, for a single scatter point (cone-beam vertex point). In a realistic detector a much smaller number of scatter events for each vertex point is expected. Large total event counts are obtained when combining a manifold of scatter points in a subsequent cone-beam reconstruction procedure.

For simplicity a single volume detector is assumed where the primary and secondary event are detected anywhere within the volume. As a result all possible ω_2 can be concidered. Boundary effects or measurement errors have not been simulated. In figure 7 the reconstruction of an artificial source is demonstrated. The original cone-beam projections as well as its reconstruction are shown as they project on a 1m square plane at 1m distance from the vertex point of the cone-beams, left and center panels. The line width of the cross shown in the figure is 7.7 cm. This corresponds in the center of the image to an angle of about 2.4^o. Polynoms up to order $T = 100$ have been used in $R(\omega, \omega_2)$. This corresponds to an angular resolution of $\Delta\omega = 1.8^o$. For comparison, a naive back-projection without filtering is shown on the right panel. There, a Compton event was projected back by adding contributions from all events that take on an angle $\omega_2 \pm \Delta\omega$ to a given pixel. The total contribution of an event to the

image should be constant. Therefore, the contributions to the summation are normalized by the length of the circle a cone-surface traces on the unit sphere, i.e. we normalize the contribution of an event by $\sin^2 \omega_2$.

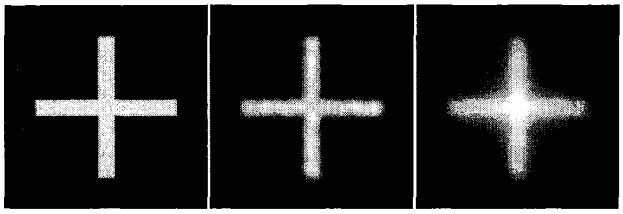

Figure 7: Approximately $500,000$ Compton scattering events have been simulated assuming an idealized noise free detector and the Klein-Nishina scatter distribution at $h\nu = 140KeV$. Left: Sampled source distribution as projected on a 1m square plane at 1m distance from the vertex point of the cone-beams. The events are binned in a 100x100 grid with pixel size corresponding to 1 cm. Center: reconstructed source using polynoms up to order $T = 100$ corresponding to an angular resolution of 1.8^o. Right: Naive back-projection reconstruction with the same 1.8^o resolution.

VII. Summary

An analytic technique for reconstruction of cone-beam projections from cone-surface projections has been derived. This linear procedure is applicable to an idealized detector, where the distribution of detected scatter angles is independent of the orientation of the incident primary γ-quantum. The proposed technique goes beyond previous analytic approaches also in that it takes into account measurement errors which vary from event to event (a typical feature of real Compton scatter detectors).

A filtered back-projection procedure is used for reconstruction. With this procedure, every volume element in the detector is assigned a two dimensional angular space. For every scattering event in a particular volume element, an event response function is added in the angular space of the volume element. These summed response functions yield the cone-beam projections of the three dimensional source on that volume element. This procedure is repeated for all volume elements within the detector. The resulting angular distributions are then used as input data for cone-beam algorithms, in order to reconstruct the 3D source distribution.

Detector geometry determines the effective angular distribution of scatter angles, which in turn determines the exact shape of the event-response function. The procedure for computing the event response function for a given angular distribution has been outlined, and is given for the Klein-Nishina scatter distribution. A procedure for computing event response functions under the condition of varying measurement errors has also been outlined.

VIII. Acknowledgements

I would like to thank Heidi Peterson for excellent editing work on this manuscript. I'm grateful to Frank Sauer for reviewing some of the arguments in the early stages of this work. Thanks is also due to Clay Spence for his suggestions on how to solve the integral in Eq. (35). I thank also Kwok Tam for presenting this work at the 1999 Medical Imaging Conference in Seatle, Washington.

IX. Appendix

A. *Convolution Theorem for Spherical Harmonics*

The convolution theorem for spherical harmonics is presented here. Consider a function $f(\Omega)$ defined in the angular space of polar coordinates $\Omega \in [0, 2\pi) \times [0, \pi)$. Since the spherical harmonics $Y_{lm}(\Omega)$ represent an orthogonal basis set spanning a complete function space, $f(\Omega)$ can be expanded in the form:

$$f(\Omega) = \sum_{l=0}^{\infty} \sum_{m=-l}^{m=l} F_{lm} Y_{lm}(\Omega) \, F_{lm} = \int d\Omega Y^*_{lm}(\Omega) f(\Omega) \,, \tag{41}$$

where the F_{lm} denote expansion coefficients of f, and the Y^*_{lm} are the complex conjugate spherical harmonics [18], defined in terms of the extended Legendre polynomials $P^m_n(\cos\omega)$:

$$Y^*_{lm}(\omega, \varphi) = (-1)^m \left[\frac{(2n+1)}{4\pi} \frac{(n-m)!}{(n+m)!} \right]^{\frac{1}{2}} P^m_n(\cos\omega) e^{im\varphi} \,. \tag{42}$$

Similarly, a function $h(\cos\omega)$ defined for $\omega \in [0, \pi)$ can be expanded in the basis of orthogonal Legendre polynomials $P_n(\cos\omega)$,

$$h(\cos\omega) = \sum_{n=0}^{\infty} H_n P_n(\cos\omega) \,, \tag{43}$$

where H_n are defined as in Eq.(14). Expanding both sides of Eq. (10), we obtain:

$$F_{lm} = \int d\Omega_2 Y^*_{lm}(\Omega_2) \int d\Omega_1 g(\Omega_1) h(\cos\omega) \tag{44}$$

$$= \int d\Omega_1 g(\Omega_1) \int d\Omega_2 Y^*_{lm}(\Omega_2) \sum_{n=0}^{\infty} H_n P_n(\cos\omega) \tag{45}$$

$$= \int d\Omega_1 g(\Omega_1) \int d\Omega_2 Y^*_{lm}(\Omega_2) \sum_{n=0}^{\infty} H_n \frac{4\pi}{2n+1} \sum_{k=-n}^{n} Y^*_{nk}(\Omega_2) Y_{nk}(\Omega_1) \tag{46}$$

$$= \sum_{n=0}^{\infty} H_n \frac{4\pi}{2n+1} \sum_{k=-n}^{n} G_{nk} \int d\Omega_2 Y^*_{lm}(\Omega_2) Y_{nk}(\Omega_2) \tag{47}$$

$$= \sum_{n=0}^{\infty} H_n \frac{4\pi}{2n+1} \sum_{k=-n}^{n} G_{nk} \delta_{ln} \delta_{mk} \tag{48}$$

$$= H_l \frac{4\pi}{2l+1} G_{lm} \,. \tag{49}$$

The following relation between spherical harmonics and Legendre polynomials has been used in line (46) above [18]:

$$P_l(\cos\omega) = \frac{4\pi}{2l+1} \sum_{m=-l}^{m=l} Y^*_{lm}(\Omega_2) Y_{lm}(\Omega_1) . \qquad (50)$$

Eq. (49) above gives the convolution theorem for spherical harmonics expansion.

If the distribution $g(\Omega_1)$ has limited bandwidth T, then coefficients higher than order T vanish, i.e., $G_{lm} = 0$ for $l > T$. Likewise, the convolved distribution will have vanishing coefficients for order $l > T$.

B. Spherical deconvolution with Legendre Polynomials

Derivation of the deconvolution formula of Eq.(12) is presented here. This deconvolution formula can be used to invert Eq. (10), directly in the original angle space, instead of in the discrete space of the expansion coefficients, as suggested by Eq.(49) above. In order to derive the deconvolution formula, first divide Eq.(49) above by $H_l \frac{4\pi}{2l+1}$:

$$G_{lm} = \frac{2l+1}{4\pi H_l} F_{lm} , \qquad (51)$$

then transform the equation back into the original angle space:

$$g(\Omega_1) = \sum_{l=0}^{\infty} \sum_{m=-l}^{l} \frac{2l+1}{4\pi H_l} F_{lm} Y_{ml}(\Omega_1) \qquad (52)$$

$$= \sum_{l=0}^{\infty} \frac{2l+1}{4\pi H_l} \sum_{m=-l}^{l} \int d\Omega_2 F(\Omega_2) Y^*_{lm}(\Omega_2) Y_{lm}(\Omega_1) \qquad (53)$$

$$= \sum_{l=0}^{\infty} \left(\frac{2l+1}{4\pi}\right)^2 \frac{1}{H_l} \int d\Omega_2 F(\Omega_2) P_l(\cos\omega) . \qquad (54)$$

This formula can be used to accomplish the deconvolution for spherical harmonics specified in Eqs.(12)-(14). Note that, based on the argument in Appendix A, the summation in this deconvolution can be truncated at T.

X. References

[1] R. Todd, J. Nightingale, and D. Everett, "A proposed Gamma camera," *Nature*, vol. 251, pp. 132–134, 1974.

[2] David Doria and Manbir Singh, "Comparison of reconstruction algorithms for an electronically collimated gamma camera," *IEEE Transaction on Nuclear Science*, vol. NS-29, no. 1, pp. 447–451, 1982.

[3] Ricardo Brechner and Manbir Singh, "Iterative reconstruction of electronically collimated SPECT images," *IEEE Transactions on Nuclear Science*, vol. 37, no. 3, pp. 1328–1332, 1990.

[4] Tom Hebert, Richard Leahy, and Manbir Singh, "Three-dimentional maximum-likelihood reconstruction for an electronically collimated single-photon-emission imaging system," *Optical Society of America*, vol. 7, no. 7, pp. 1305–1313, 1990.

[5] Manbir Singh, "An electronically collimated gamma camera for single photon emission computed tomography. Part 1: Theoretical considerations and design criteria," *Medical Physics*, vol. 10, no. 4, pp. 421–427, 1983.

[6] C. Sauve, Anne, O. Hero III, Alfred, and W. Rogers, Leslie, "3D image reconstruction for a Compton SPECT camera model," *IEEE Trans. Nuclear Science*, vol. 46, no. 6, pp. 2075–2084, November 1999.

[7] H. Barrett, L. Parra, and T. White, "List-mode likelihood," *Journal of the Optical Society of America A*, vol. 14, no. 11, 1997.

[8] L. Parra and H. Barrett, "List-mode likelihood: EM algorithm and image quality estimation demonstrated on 2-D PET," *IEEE Trans. Medical Imaging*, vol. 17, no. 2, pp. 228–235, Apr. 1998.

[9] Waclaw Krzyzanowski, "Compton lens formula: A new way of recunstructing single-gamma emission images," Tech. Rep. Si-85-16, Physics Department, Siegen University, Siegen, Germany, 1985.

[10] J. Cree, Michael and J. Bones, Philip, "Towards direct reconstruction from gamma camera based on Compton scattering," *IEEE Transaction on Medical Imaging*, vol. 13, no. 2, pp. 398–407, 1994.

[11] R. Basko, G. Zeng, and G. Gullberg, "Application of spherical harmonics to image reconstruction for the Compton camera," *Phys. Med. Biol.*, vol. 43, pp. 887–894, 1998.

[12] F. Noo, R. Clack, and M. Defrise, "Cone-beam reconstruction from general discrete vertex sets using Radon rebinning algorithms," *IEEE Trans. Nuclear Science*, vol. 44, no. 3, pp. 1309–1316, June 1997.

[13] S. Schaller, T. Flohr, and P. Steffen, "An efficient Fourier method for 3-D Radon inversion in exact cone-beam CT reconstruction," *IEEE Trans. on Medical Imaging*, vol. 17, no. 2, pp. 244–250, Apr. 1998.

[14] K.C. Tam, S. Samarasekera, and F. Sauer, "Exact cone beam CT with a spiral scan," *Physics in Medicine and Biology*, vol. 43, no. 4, pp. 1015–1024, Apr. 1998.

[15] F. Noo, R. Clack, and M. Defrise, "Direct reconstruction of cone-beam data acquired with a vertex path containing a circle," *IEEE Trans. Image Processing*, vol. 7, no. 6, pp. 854–867, June 1998.

[16] Harrison Barrett and William Swindell, *Radiological imaging*, vol. I and II, Academic Press, 1981.

[17] Harrison Barrett and William Swindell, "Analog reconstruction methods for transaxial tomography," *Proceedings of the IEEE*, vol. 65, no. 1, pp. 89–107, 1977.

[18] J.D. Jackson, *Classical Electrodynamics*, John Wiley & Sons, 1975.